Potential Energy Surface and Product Branching Ratios for the Reaction of $C(^3P_j)$ with the Allyl Radical: An ab Initio/RRKM Study

T. L. Nguyen,[†,‡] A. M. Mebel,[*,†] and R. I. Kaiser[§]

Institute of Atomic and Molecular Sciences, Academia Sinica, P.O. Box 23-166, Taipei 10764, Taiwan, and Department of Chemistry, University of Hawai'i—Manoa, Honolulu, Hawaii 96822-2275

Received: January 12, 2003; In Final Form: February 19, 2003

Ab initio G2M(MP2)//B3LYP/6-311G** calculations have been carried out to investigate the potential energy surface for the $C(^3P_j) + C_3H_5(X\ ^2A_1)$ reaction. The results show that $C(^3P_j)$ can add without a barrier either to a terminal CH_2 group of the allyl radical to form a metastable intermediate INT1 or between two CH_2 groups to produce a bicyclic structure INT2. INT1 immediately isomerizes to buta-1,3-dien-4-yl (INT3), which can decompose to vinylacetylene + H or to the vinyl radical + acetylene. Buta-1,3-dien-4-yl (INT3) can also rearrange to 1,2-dien-4-yl (INT4), and the latter fragments by the H atom loss to vinylacetylene or butatriene. The alternative pathway from the reactants to 1,2-dien-4-yl (INT4) involves two sequential ring openings in the bicyclic intermediate INT2. 1,2-dien-4-yl (INT4) can also rearrange to but-2-yn-1-yl (INT7), which in turn decomposes to butatriene + H. The RRKM theory has been applied to compute rate constants for unimolecular reaction steps and the product branching ratios. Vinylacetylene + H and vinyl radical + acetylene are predicted to be the major reaction products, and their branching ratios strongly depend on the initial branching between the intermediates INT1 and INT2 varying between 29.8/69.8 for 100% of INT1 to 62.4/35.7 for 100% of INT2. Butatriene + H are expected to be the minor products, while the other product channels are much less favorable according to the calculated energies and rate constants.

1. Introduction

Bimolecular reactions of ground-state carbon atoms, $C(^3P_j)$, with unsaturated hydrocarbons and their radicals are of great importance in hydrocarbon syntheses, combustion processes, and interstellar chemistry. Atomic carbon is the fourth most abundant element in universe and is ubiquitous in the interstellar medium. Carbon atoms have been detected via their 609 μm $^3P_1-^3P_0$ transition in significant amounts in, for instance, circumstellar envelopes of the carbon stars IRC+10216 and α Orionis,[1−4] toward the proto planetary nebulae CRL 618 and CRL 2688,[5] in the diffuse cloud ζOph,[6] and toward the dense cloud OMC-1.[7] In terrestrial environments such as oxidative hydrocarbon flames, the transient carbon atoms are also assumed to contribute significantly to combustion processes.[8] On the other hand, the allyl radical CH_2CHCH_2 is the simplest conjugated π-electron hydrocarbon radical and is the prototype for an extended conjugated system with odd number of electrons. It plays important roles in many combustion,[9] photochemical,[10] and thermal reactions.[11] As both atomic carbon and allyl radical can be present in hydrocarbon flames or in other terrestrial and extraterrestrial environments, they may react with each other producing various more stable hydrocarbon species.

In a series of our recent experimental and theoretical works,[12] we investigated reactions of $C(^3P_j)$ with various unsaturated hydrocarbons and found that the carbon/hydrogen exchange channel,

$$C(^3P_j) + C_nH_m \rightarrow C_{n+1}H_{m-1} + H(^2S_{1/2})$$

dominates most of these reactions. In this view, one can expect that the reaction of $C(^3P_j)$ with CH_2CHCH_2 should produce some C_4H_4 isomers and hydrogen atoms. On the other hand, many other product channels including $C_4H_3 + H_2$, $C_2H_3 + C_2H_2$, $CH_4 + C_3H$, $C_3H_2 + CH_3$, etc., are highly exothermic and cannot be ruled out a priori. Therefore, a careful and detailed study of potential energy surface (PES) for the $C(^3P_j) + CH_2CHCH_2$ system is required in order to elucidate possible reaction mechanisms leading to various products and to predict potential relative branching ratios of different products.

Experimental difficulties to simultaneously produce high-intensity supersonic beams of carbon atoms and allyl radicals in a crossed-beam setup have eluded the $C(^3P_j) + CH_2CHCH_2$ reaction from being studied experimentally so far. In this paper, we report a high-level ab initio study of potential energy surface for this reaction, the energetics and molecular structures of its intermediates, products, and transition states, then use the ab initio results to calculate rate constants for individual unimolecular reaction steps and relative yields (branching ratios) of various products, and consider astrophysical implications which follow.

2. Computational Methods

The geometry of the reactants, products, intermediates, and transition states has been optimized by employing the hybrid density functional B3LYP method[13,14] with the 6-311G** basis set. Vibrational frequencies, calculated at the same B3LYP/6-311G** level, were used for characterization of the stationary points (number of imaginary frequencies NIMAG = 0 and 1 for local minima and transition states, respectively) and zero-point energy corrections (ZPE). To obtain more accurate energies, we used the G2M(MP2) computational scheme,[15] which approximates coupled-cluster CCSD(T) calculations[16] with the large 6-311+G(3df,2p) basis set. The G2M(MP2)//

* To whom correspondence should be addressed.
† Institute of Atomic and Molecular Sciences.
‡ Present address: Division of Physical and Analytical Chemistry, Department of Chemistry, University of Leuven, Belgium.
§ Department of Chemistry.

10.1021/jp034074j CCC: $25.00
Published on Web 03/27/2003

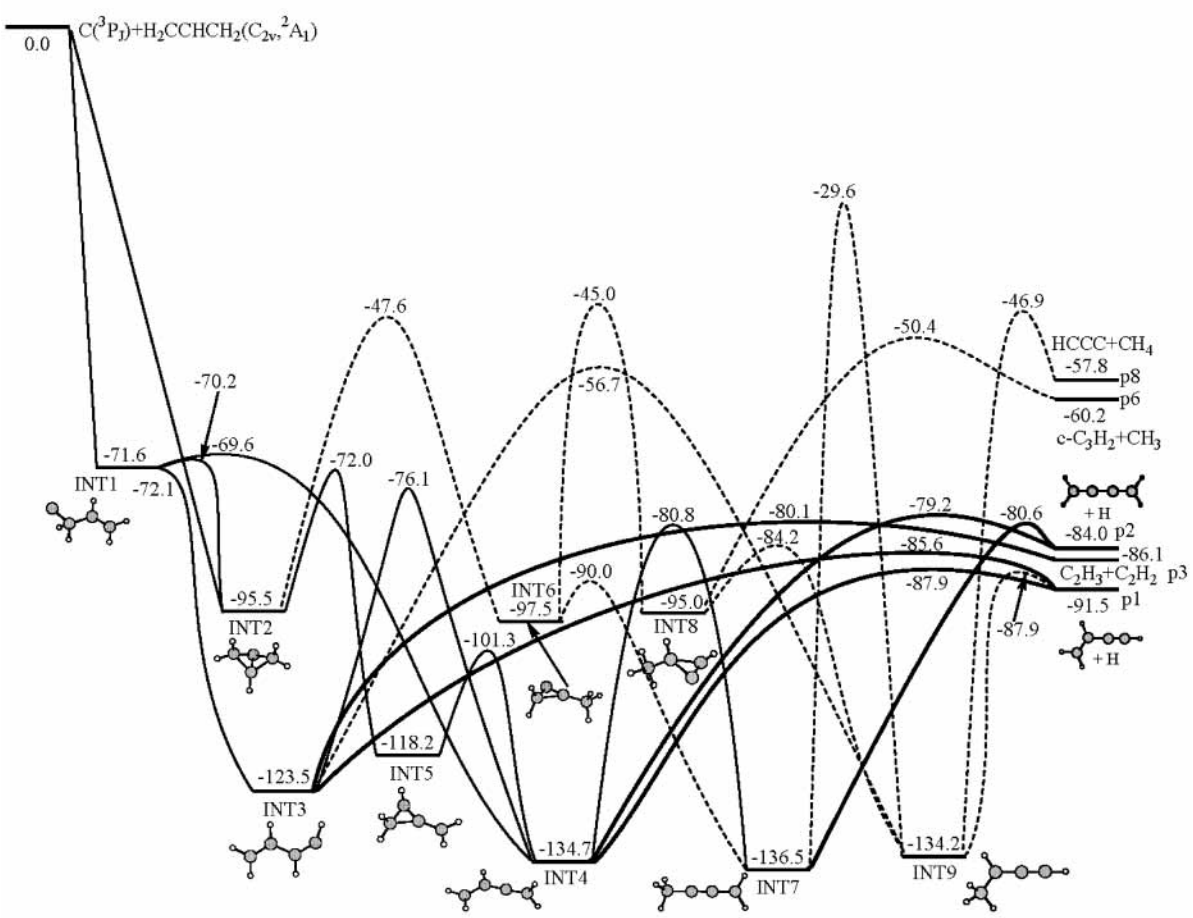

Figure 1. Profile of PES of the $C(^3P_j) + C_3H_5(X\ ^2A_1)$ reaction calculated at the G2M(MP2)//B3LYP/6-311G** + ZPE(B3LYP/6-311G**) level. The relative energies are given in kcal/mol. Plain and dashed lines show significant and insignificant reaction channels, respectively, and bold lines show most important decomposition pathways.

B3LYP/6-311G** + ZPE(B3LYP/6-311G**) calculational approach is expected to provide accuracies of 1−2 kcal/mol for relative energies of various stationary points on PES including transition states. The GAUSSIAN 98[17] and MOLPRO 2000[18] programs were employed for the calculations.

We used the RRKM theory for computations of rate constants of individual reaction steps.[19−21] Rate constant $k(E)$ at an internal energy E for a unimolecular reaction A* → A# → P can be expressed as

$$k(E) = \frac{\sigma W^{\neq}(E - E^{\neq})}{h \quad \rho(E)}$$

where σ is the reaction path degeneracy, h is the Planck constant, $W^{\#}(E - E^{\#})$ denotes the total number of states for the transition state (activated complex) A# with a barrier $E^{\#}$, $\rho(E)$ represents the density of states of the energized reactant molecule A*, and P is the product or products. The total number of states and density of states were computed using the direct count method.[22] It should be noted that we used the harmonic approximation to calculate the total number and density of states. For the case in which the excitation energy is large and there exist low-frequency modes, the harmonic approximation will not be accurate for low-frequency modes in calculating these quantities and may introduce certain errors in our treatment. To take into account anharmonicity, more sophisticated RRKM calculations are required, but they are beyond the scope of the present work.

Assuming single-collision conditions for the reaction, master equations for unimolecular reactions can be expressed as follows:

$$\frac{d[C]_i}{dt} = \sum k_n[C]_j - \sum k_m[C]_i$$

where $[C]_i$ and $[C]_j$ are concentrations of various intermediates or products and k_n and k_m are microcanonical rate constants computed using the RRKM theory. The fourth-order Runge−Kutta method[21] was employed to solve the master equations and to obtain numerical solutions for the concentrations of various products versus time. The concentrations at the times when they have converged were used for calculations of the product branching ratios.

3. Results and Discussion

PES for the $C(^3P_j) + C_3H_5(X^2A_1)$ reaction is shown in Figure 1, while optimized geometries for various intermediates and transition states are illustrated in Figures 2 and 3, respectively. Total energies, ZPE, and relative energies of various species are collected in Table 1.

3.1. Initial Reaction Steps and Isomerization Pathways of the C_4H_5 Radical. The reaction depicts two barrierless entrance channels. The initial step of the reaction of atomic carbon $C(^3P_j)$ with the allyl radical $C_3H_5(X^2A_1)$ can lead to two different intermediates (Figure 1). INT1, CCH_2CHCH_2, is produced by the atomic carbon addition to the terminal carbon atom of allyl without an entrance barrier and is stabilized by 71.6 kcal/mol relative to the reactants. On the other hand, a bicyclic intermediate INT2, 95.5 kcal/mol below $C(^3P_j) + C_3H_5$-

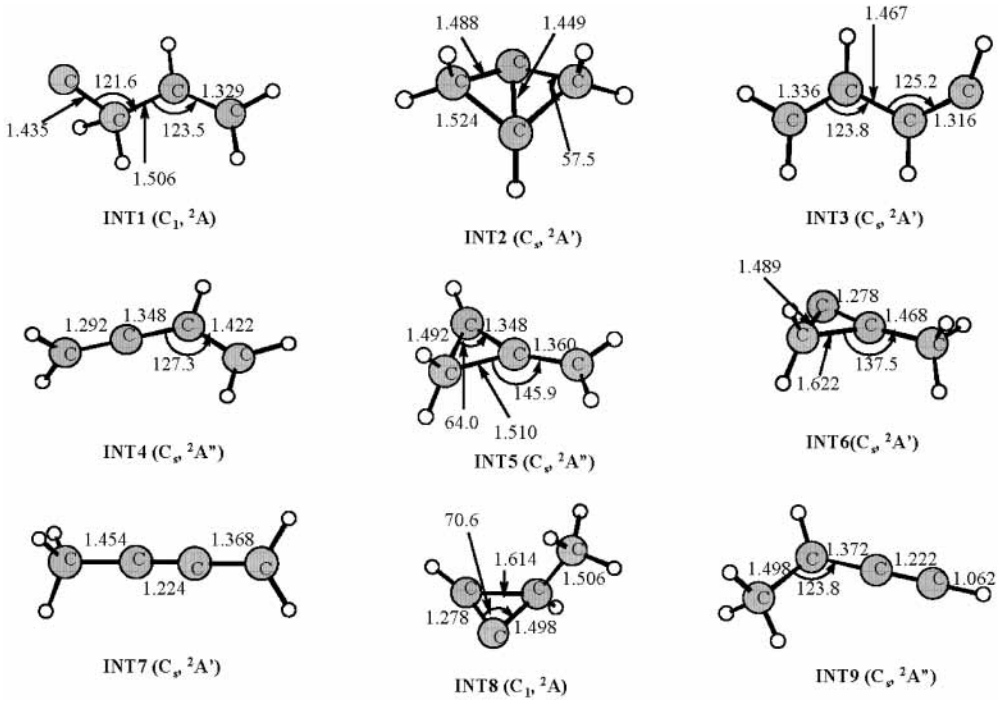

Figure 2. B3LYP/6-311G(d,p)-optimized geometries of various intermediates for the $C(^3P_j) + C_3H_5(X\ ^2A_1)$ reaction. (Bond lengths are in angstroms; bond angles are in degrees).

(X^2A_1), is formed by the carbon addition between two terminal CH_2 groups of allyl, also without a barrier. A third possibility is addition of the carbon atom to the C−C bond, which is common for the reactions of $C(^3P_j)$ with olefins and their radicals.[12] However, in the case of the allyl radical such addition does not take place. We tried to locate a C_4H_5 isomer with C added to the C−C bond, i.e., a three-member ring (CH_2CCH)-CH_2 structure with an out-of-ring CH_2 group, but optimizations started from slightly different initial structures converged to INT1 or INT2. Hence, we concluded that only these two isomers can be formed at the initial reaction step.

INT1 appeared to be metastable and can readily undergo a 1,2-H shift to the terminal carbenic carbon, forming the H_2-CCHCHCH intermediate INT3 (buta-1,3-dien-4-yl). The INT1 → INT3 transition state exists at the B3LYP level of theory, but at the higher G2M level its energy is 0.5 kcal/mol lower than that of INT1, indicating that the hydrogen shift occurs (similar to the reactions of atomic carbon with two other hydrocarbon radicals vinyl[23] and propargyl[24]) virtually without a barrier. INT3 resides 123.5 kcal/mol below the reactants. INT1 can also depict an insertion of the carbenic carbon into the neighboring carbon−carbon bond, yielding intermediate INT4, $H_2CCHCCH_2$ or buta-1,2-dien-4-yl. The INT1 → INT4 barrier is only 2.0 kcal/mol, and INT4 is located 134.7 kcal/mol lower in energy than $C(^3P_j) + C_3H_5(X^2A_1)$. One can imagine another pathway leading from the reactants to INT4, the atomic carbon addition to the carbon−carbon bond of allyl, forming a cyclic intermediate followed by the three-member ring opening, similar to the reaction of carbon atoms with olefines. However, as was mentioned above, a $(CH_2CCH)CH_2$ cyclic structure is not a local minimum on the PES. Since INT1 is a metastable species, one cannot exclude that some descending trajectories exist on the surface leading from the reactants to INT4, where the atomic carbon approaches a terminal carbon atom of allyl or the carbon−carbon bond. The third channel of isomerization of INT1 involves rotation around the $C-CH_2C$ bond, resulting in the bicyclic structure INT2. The calculated barrier is 1.4 kcal/mol and the INT1 → INT2 rearrangement is 23.9 kcal/mol exothermic, so that the reverse barrier is 25.3 kcal/mol. In the forward direction, the INT1 → INT2 isomerization occurs by rotation about a single C−C bond and the barrier is low, but in the reverse direction the reaction involves a cleavage of two C−C bonds in the bicycle and the barrier is significant. Opening of one of the rings in INT2 yields another cyclic intermediate INT5 via a barrier of 23.5 kcal/mol. INT5 is positioned 118.2 kcal/mol below the reactants and can undergo the second ring opening, leading to INT4 with a barrier of 16.9 kcal/mol. Thus, INT5 can be also formed from the initial reactants via intermediates INT1 and INT4. Intermediates INT3 and INT4 can rearrange to each other by 1,2-H migration from CH to the terminal CH group in the former or from the terminal CH_2 group to the hydrogen-free C atom in the latter. The calculated barrier is rather high, 47.4 and 58.6 kcal/mol in the INT3 → INT4 and INT4 → INT3 directions, respectively, but still the corresponding transition state lies 76.1 kcal/mol below the reactants.

The 1,2-H migration from CH to CH_2 in the bicyclic intermediate INT2 accompanied with a cleavage of the $HC-CH_2$ bond gives a three-member structure INT6 with an out-of-ring CH_3 fragment. INT6 is 2.0 kcal/mol more stable than INT2 and lies 97.5 kcal/mol lower in energy than the initial reactants. The H shift barrier for the INT2→INT6 isomerization is calculated as 47.9 kcal/mol. Next, the ring opening in INT6 leads to intermediate INT7 over a low barrier of 7.5 kcal/mol. INT7, H_3CCCCH_2 or but-2-yn-1-yl, is the most stable isomer of the C_4H_5 radical and resides 136.5 kcal/mol lower in energy than the reactants, $C(^3P_j) + C_3H_5(X^2A_1)$. Alternatively, INT7 can be produced from INT4 by 1,2-hydrogen migration from CH to the neighboring terminal CH_2 group via a barrier of 53.9 kcal/mol. The other rearrangement pathway for INT6 involves the H migration between two ring carbons, one connected to two hydrogen atoms and the other bound to the external CH_3 group. This migration gives another three-member cyclic intermediate INT8, which lies 2.5 kcal/mol above INT6 and 95.0 kcal/mol lower in energy than the reactants. The INT6 → INT8 barrier height has a value of 52.5 kcal/mol, typical for the 1,2-H shift. INT8 can ring-open and form intermediate INT9

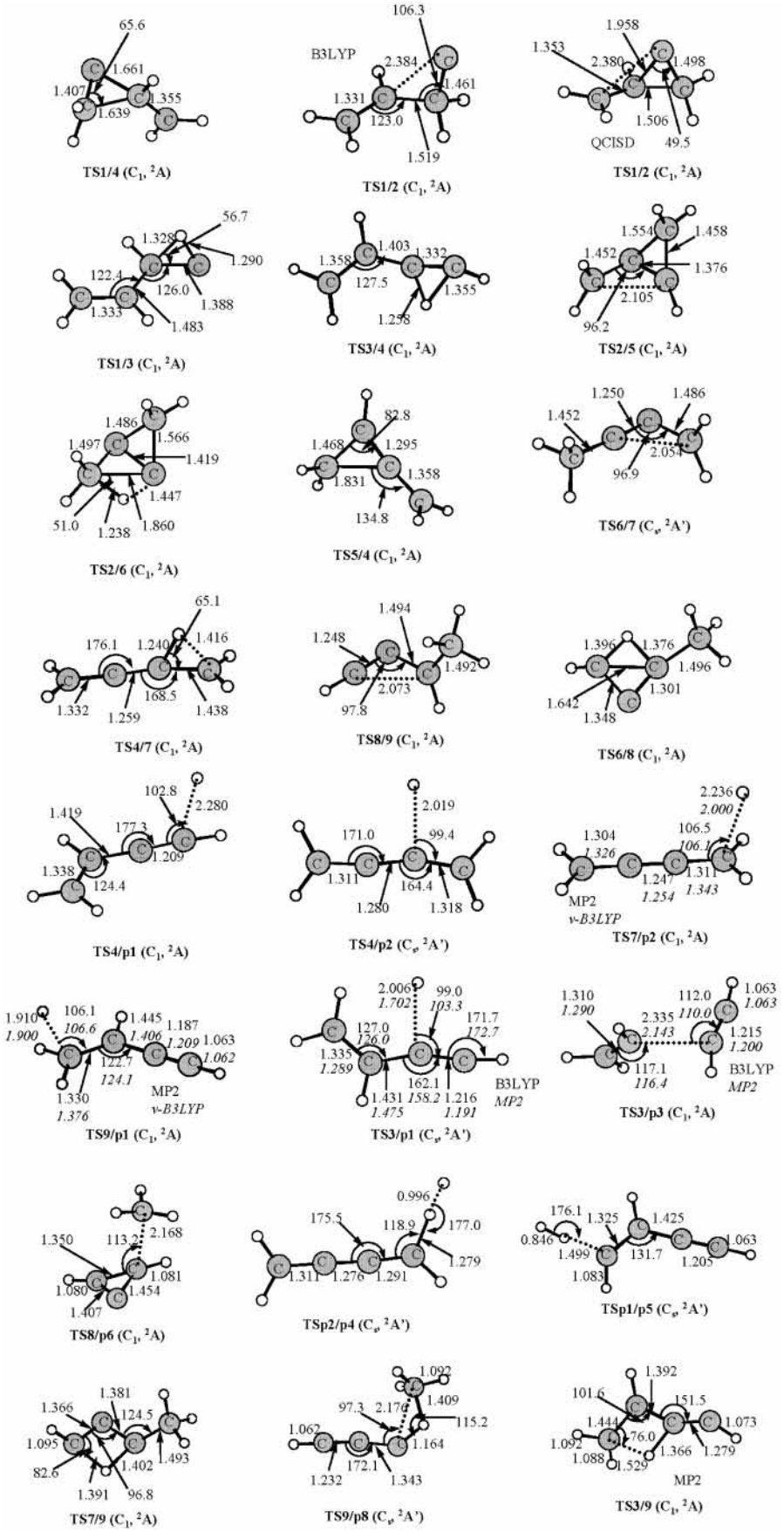

Figure 3. B3LYP/6-311G(d,p)-optimized geometries of various transition states for the $C(^3P_j) + C_3H_5(X\ ^2A_1)$ reaction. (Bond lengths are in angstroms; bond angles are in degrees).

overcoming a 10.8 kcal/mol barrier. INT9 lies 134.2 kcal/mol below $C(^3P_j) + C_3H_5(X^2A_1)$ and has a $H_3CCHCCH$ but-1-yn-3-yl structure. Another isomerization pathway connects INT9 with INT3 through the 1,3-hydrogen shift from CH to CH_2 in

TABLE 1: Total Energies (hartrees), Zero-Point Energies, and Relative Energies (kcal/mol) for Various Species Calculated at the B3LYP/6-311G and G2M(MP2) Levels of Theory**

species	total energy		ZPE	Relative energy	
	B3LYP	G2M[a]		B3LYP	G2M
$C(^3P_j) + H_2CCHCH_2(X\ ^2A_1)$	−155.15212	−154.80822	41.31	0.0	0.0
INT1	−155.26251	−154.92236	43.10	−67.5	−71.6
INT2	−155.30064	−154.96040	45.76	−88.7	−95.5
INT3	−155.34895	−155.00509	44.60	−120.2	−123.5
INT4	−155.37086	−155.02288	43.90	−134.7	−134.7
INT5	−155.34237	−154.99651	44.03	−116.7	−118.2
INT6	−155.30567	−154.96353	44.77	−92.9	−97.5
INT7	−155.37308	−155.02576	43.50	−136.5	−136.5
INT8	−155.30030	−154.95961	44.50	−89.8	−95.0
INT9	−155.36733	−155.02208	43.70	−132.7	−134.2
p1: $H_2C{=}CHC{\equiv}CH(^1A') + H(^2S)$	−155.28296	−154.95400	38.23	−85.2	−91.5
p2: $H_2C{=}C{=}C{=}CH_2(^1A_g) + H(^2S)$	−155.27733	−154.94212	37.56	−82.3	−84.0
p3: $C_2H_3(^2A') + C_2H_2(^1\Sigma_g^+)$	−155.28173	−154.94535	39.73	−82.9	−86.1
p4: $H_2CCCCH(^2A') + H_2(^1\Sigma_g^+)$	−155.29516	−154.95724	34.63	−96.4	−93.5
p5: $HCCHCCH(^2A') + H_2(^1\Sigma_g^+)$	−155.26990	−154.94015	35.94	−79.3	−82.8
p6: $c\text{-}C_3H_2(^1A_1) + CH_3(^2A_2'')$	−155.23723	−154.90410	38.70	−56.0	−60.2
p7: $c\text{-}C_3H(^2B_2) + CH_4(^1A_1)$	−155.24253	−154.90413	39.97	−58.1	−60.2
p8: $l\text{-}C_3H(^2\Pi) + CH_4(^1A_1)$	−155.24236	−154.90033	38.54	−59.4	−57.8
p9: $HCCCH(^3B) + CH_3(^2A_2'')$	−155.22545	−154.88442	34.46	−52.9	−47.8
p10: $H_2CCC(^1A_1) + CH_3(^2A_2'')$	−155.21836	−154.88320	37.94	−44.9	−47.1
p11: $H_2CCCH(^2B_1) + CH_2(^3B_1)$	−155.20183	−154.87730	29.33	−43.2	−43.4
TS1/4	−155.25931	−154.91915	43.05	−65.5	−69.6
TS1/2	−155.25995	−154.92014	43.28	−65.7	−70.2
TS1/3	−155.26022	−154.92309	41.26	−67.9	−72.1
TS3/4	−155.27337	−154.92947	40.90	−76.5	−76.1
TS2/5	−155.26339	−154.92290	43.15	−68.0	−72.0
TS2/6	−155.21998	−154.88414	42.52	−41.4	−47.6
TS5/4	−155.31427	−154.96972	42.32	−100.7	−101.3
TS6/7	−155.29333	−154.95158	42.76	−87.2	−90.0
TS4/7	−155.28300	−154.93691	39.95	−83.5	−80.8
TS8/9	−155.28294	−154.94245	42.53	−80.9	−84.2
TS6/8	−155.21727	−154.88000	41.10	−41.1	−45.0
TS7/9	−155.19476	−154.85536	39.97	−28.1	−29.6
TS3/9		−154.89857[b]	38.33[c]		−56.7
TS4/p1	−155.28881	−154.94832	39.50	−87.6	−87.9
TS4/p2	−155.27436	−154.93443	38.47	−79.5	−79.2
TS7/p2[d]	−155.28260	−154.93660	38.66	−84.5	−80.6
TS9/p1[d]	−155.28881	−154.94832	39.50	−87.6	−87.9
TS3/p1	−155.27813	−154.94465	39.04	−81.3	−85.6
TS3/p3	−155.27451	−154.93585	40.52	−77.6	−80.1
TS8/p6	−155.22708	−154.88861	41.00	−47.4	−50.4
TS9/p8	−155.22329	−154.88290	38.98	−47.0	−46.9
TSp2/p4	−155.26830	−154.92243	35.77	−78.4	−71.7
TSp1/p5	−155.26226	−154.92570	36.73	−73.7	−73.7

[a] "Higher level corrections" (HLC) are included. [b] Based on the MP2/6-311G**-optimized geometry. [c] Calculated at the MP2/6-311G** level of theory and scaled by 0.95. [d] Based on the G2M(MP2)//variational B3LYP/6-311G** calculations. See text for the detailed description.

the latter. We were able to locate the corresponding TS3/9 transition state only at the MP2/6-311G** level, while the B3LYP saddle-point optimization failed. Within the G2M//MP2/6-311G** approximation, TS3/9 lies 56.7 kcal/mol lower in energy than the reactants, so that the barrier height is 66.8 and 77.1 kcal/mol in the forward and reverse directions, respectively. To confirm that a first-order saddle point actually exists on the INT3→INT9 pathway, it is necessary to perform the transition state optimization at a higher level, for example, QCISD/6-311G**. However, according to the G2M//MP2/6-311G** calculations, the barrier is expected to be significantly higher than those for the other isomerization pathways for INT3 and INT9, and therefore we did not carry out more accurate calculations. Finally, INT9 can be produced from INT7 by 1,3-H migration from the CH_3 group to the hydrogen-free C atom connected to CH_2. However, the barrier in this case is very high and exceeds 100 kcal/mol in both directions.

We can compare relative stabilities of some C_4H_5 isomers obtained here at the G2M level of theory with those reported earlier by Parker and Cooksy.[25] According to both our and their studies, but-2-yn-1-yl (INT7) is the most stable isomer. At the G2M level, buta-1,2-dien-4-yl (INT4) and but-1-yn-3-yl (INT9) lie 1.8 and 2.3 kcal/mol higher in energy than INT7. At the CCSD(T)/6-311G** level, the relative energetic order of INT4 and INT9 is different; they reside 2.3 and 1.9 kcal/mol, respectively, above INT7. Similar values were obtained in the QCISD and CCSD(T) calculations by Parker and Cooksy.[25] However, the basis set correction in the G2M scheme makes buta-1,2-dien-4-yl slightly more stable than but-1-yn-3-yl. We can conclude that the INT4 and INT9 isomers of the C_4H_5 radical are very close in energy and lie about 2 kcal/mol higher in energy than the most stable but-2-yn-1-yl structure INT7. Also, according to our calculations, buta-1,3-dien-4-yl INT3 is 13.0 kcal/mol higher in energy than INT7: this is close to the CCSD(T) result of Parker and Cooksy of 12.3 kcal/mol.[25]

Summarizing the C_4H_5 isomerization mechanisms and barrier heights, we can see that the rearrangements occur by ring closure/opening processes, 1,2-H shifts, and occasionally by 1,3-H migrations. The ring opening steps exhibit relatively low barriers in the range of 7−10 kcal/mol, except for the bicyclic structure INT2, which opens one of its rings to produce INT5 with a barrier of 23.5 kcal/mol. The 1,2-H shift barriers are much higher, at least about 50 kcal/mol in one direction. The only exception is the H shift in the metastable intermediate

INT1, which is virtually barrierless. Finally, 1,3-H shifts depict even higher barriers than the 1,2 shifts and are least probable.

3.2. Fragmentation of C_4H_5 Isomers. We investigate now possible fragmentation pathways of the intermediates involved in the $C(^3P_j) + C_3H_5(X\ ^2A_1)$ reaction. INT3 and INT4 can lose a hydrogen atom, producing the vinylacetylene (p1), the most stable isomer on the singlet C_4H_4 PES, and butatriene (p2). The exothermicities of the $C(^3P_j) + C_3H_5(X\ ^2A_1) \rightarrow C_4H_4(X\ ^1A')$ (p1) + $H(^2S_{1/2})$ and $C(^3P_j) + C_3H_5(X\ ^2A_1) \rightarrow C_4H_4(X\ ^1A_g)$ (p2) + $H(^2S_{1/2})$ reactions are calculated as 91.5 and 84.0 kcal/mol, respectively (89.7 kcal/mol in experiment[26] for p1). p1 is produced by a hydrogen atom elimination from INT3 and INT4 with the exit barriers of 5.9 and 3.6 kcal/mol, while p2 can be formed from INT4 via an exit barrier of 4.8 kcal/mol. Additionally, a carbon−carbon bond cleavage in INT3 yields vinyl plus acetylene (p3) with an exit barrier of 6.0 kcal/mol and the total reaction exothermicity of 86.1 kcal/mol.

INT7 can eliminate an H atom from the CH_3 group also producing butatriene p2. We were able to locate the corresponding TS7/p2 transition state only at the MP2/6-311G** level and the exit barrier (relative to the p2 + H products) is computed as 10.7 kcal/mol by the G2M//MP2/6-311G** method. On the other hand, B3LYP saddle-point optimization does not result in a transition state and shows that at this level the H loss from INT7 does not have an exit barrier. For RRKM calculations, we used the variational approach[21] scanning the PES along the breaking C−H bond and optimizing all other geometric parameters. For each partially optimized point, we calculated $3N - 7$ vibrational frequencies and these frequencies were used for calculations of the number of states for these transition state candidates. As the frequencies were projected out of the gradient direction, this procedure is as well-defined as calculations of $3N - 6$ frequencies for a stationary point. The frequencies of the parting fragments computed within this approach smoothly converge to the frequencies of separated fragments as the breaking C−H bond distance increases. Single-point energies were refined at the G2M level, and the calculations demonstrated that an exit barrier exists at the G2M//B3LYP PES. The variational transition state, the structure of which is shown in Figure 3, was chosen based on the microcanonical variational transition state theory (VTST)[21] by minimizing the number of states along the reaction coordinate C−H. Considering the position of the variational transition state, we find that the exit barrier is 3.4 kcal/mol at this G2M//variational B3LYP level.

Intermediate INT8 is a precursor of the $c\text{-}C_3H_2 + CH_3$ products. The $C(^3P_j) + C_3H_5(X\ ^2A_1) \rightarrow c\text{-}C_3H_2 + CH_3$ channel is computed to be 60.2 kcal/mol exothermic (57.5 kcal/mol in experiment[26]). The cleavage of the out-of-ring $c\text{-}CH_3$ bond in INT8 takes place with an exit barrier of 9.8 kcal/mol. Other isomers of the C_3H_2 species can be produced by the C−C bond cleavages from INT7 (vinylidenecarbene H_2CCC, $^1A_1$) and INT9 (triplet propargylene HCCCH, ^3B). The relative energies of H_2-CCC and HCCCH with respect to $c\text{-}C_3H_2$ are calculated as 13.1 and 12.4 kcal/mol (13.5 and 11.3 kcal/mol at the CCSD(T)/6-311+G(3df,2p) level[27]), respectively, and therefore the exothermicities of the $C(^3P_j) + C_3H_5(X\ ^2A_1) \rightarrow H_2CCC\ (^1A_1) + CH_3$ and $C(^3P_j) + C_3H_5(X\ ^2A_1) \rightarrow HCCCH\ (^3B) + CH_3$ reactions can be predicted as 47.1 and 47.8 kcal/mol. These values are lower than the exothermicities of the other channels shown in Figure 1, so the contribution of these products is not expected to be significant.

Hydrogen loss from the CH_3 group in INT9 produces the most stable vinylacetylene product. As for the case of the H elimination from INT7, we were able to locate the TS9/p1 transition state at the MP2/6-311G** level but not at B3LYP. Again we used the VTST calculations at the B3LYP level with refining the single point energies using the G2M method. At the G2M//variational B3LYP level the exit barrier is computed as 3.6 kcal/mol, somewhat lower than the value of 5.1 kcal/mol obtained at the G2M//MP2/6-311G** level. INT9 also serves as a precursor for the $l\text{-}C_3H + CH_4$ products. The dissociation occurs by the 1,2-H shift from CH to CH_3 in conjunction with the C−C bond cleavage. The barrier at TS9/p8 is calculated as 87.3 and 10.9 kcal/mol in the forward and reverse directions, respectively, and the $l\text{-}C_3H + CH_4$ product channel is 57.8 kcal/mol exothermic. The cyclic isomer of C_3H, which is slightly more stable than the linear $l\text{-}C_3H$ structure, can be produced by the similar mechanism from INT8. However, the INT8 → $c\text{-}C_3H + CH_4$ channel is not expected to compete with the INT8 → INT9 ring opening or even with the INT8 → $c\text{-}C_3H_2 + CH_3$ dissociation since it has exothermicity similar to that for the latter but should have a much tighter transition state than TS8/p6. Hence, we did not investigate this channel in detail.

Since the transition states corresponding to the C−H or C−C bond rupture exhibit large separations between the parting fragments implying that the interaction between them may be dominated by dispersion, one can question the applicability of the DFT B3LYP method to these transition states. To check this, we additionally performed geometry optimization for two transition states, TS3/p1 and TS3/p3, at the MP2/6-311G** level. As seen in Figure 3, the differences in the B3LYP- and MP2-optimized geometric parameters are relatively small, except for the C−H and C−C breaking bond distances, which are 0.2−0.3 Å shorter at the MP2 level. However, the PES has been found to be rather flat with respect to these parameters. For instance, the MP2 energies of TS3/p1 and TS3/p3 change upon optimization (starting from the B3LYP geometries) only by 0.75 and 0.11 kcal/mol, respectively. The barriers at TS3/p1 and TS3/p3 calculated at the G2(MP2)//MP2/6-311G** level are respectively 3.5 and 1.7 kcal/mol higher than those obtained at G2(MP2)//B3LYP/6-311G**. To conclude which geometry is more accurate, B3LYP or MP2, expensive higher-level QCISD or large-active-space CASSCF calculations would be required. However, according to the above consideration, the errors introduced by the use of the B3LYP geometries are not expected to be large.

We tried to find decomposition pathways leading to the other highly exothermic products, $n\text{-}C_4H_3(^2A') + H_2$ (p4) and $i\text{-}C_4H_3(^2A') + H_2$ (p5), for which the relative energies with respect to the initial $C(^3P_j) + C_3H_5(X\ ^2A_1)$ reactants are computed as −93.5 and −82.8 kcal/mol, respectively. INT7 and INT9 look like suitable precursors to produce *n*- and *i*-C_4H_3, respectively, by H_2 loss from the terminal CH_3 groups. However, the calculations show that the H_2 elimination does not occur − at least not on the ground-state surface. A careful search of transition states corresponding to these processes gave TSp2/p4 and TSp1/p5, which appeared to correspond to the secondary hydrogen abstraction reactions, $H_2CCCCH_2 + H$ (p2) → $n\text{-}C_4H_3(^2A') + H_2$ (p4) and $H_2CCHCCH + H$ (p1) → $i\text{-}C_4H_3(^2A') + H_2$ (p5). The former is 9.5 kcal/mol exothermic and has a barrier of 12.3 kcal/mol, while the latter is 8.7 kcal/mol endothermic and the barrier height is 17.8 kcal/mol. The reactions of the primary C_4H_4 products with H atoms can take place only if secondary collisions are possible under the reaction conditions. Therefore, $C_4H_3 + H_2$ cannot be formed as primary products of the $C(^3P_j) + C_3H_5(X\ ^2A_1)$ reaction or unimolecular decomposition of the C_4H_5 radical. This result is due to the fact that

the reverse reactions are additions of molecular hydrogen to the σ C_4H_3 radicals. We have already discussed in several occasions[24b,28,29] that an H_2 addition to a σ radical is unfavorable in terms of interaction of the singly occupied σ orbital of the radical and the antibonding σ_u orbital of H_2 and therefore first-order saddle points could not be found for this process. As a result, the H_2 addition has to follow the two-step mechanism, hydrogen atom abstraction from H_2 by the radical and then addition of the second H atom to the closed-shell species formed at the first step. This behavior was earlier found for $C_2H_3(^2A')$,[28] $C_2H(^2\Sigma^+)$,[30] $C_4H(^2\Sigma^+)$,[24b] and $HCCH(^3B_2)$,[29] and now the C_4H_3 radical can be added to this list.

For other product channels, INT4 could be a precursor for $C_3H_3(^2B_1) + CH_2(^3B_1)$ and for $H_2CCCH_2(^1A_1) + CH(^2\Pi)$, INT7 and INT9 could in principle decompose to $H_3CCCH(^1A_1) + CH(^2\Pi)$ after a 1,2-hydrogen shift and the corresponding C−C bond cleavage, and the H migration from CH_3 to the neighboring CH group in INT9 followed by (or accompanied with) the cleavage of the adjacent C−C bond may give $C_2H_4(^1A_g) + C_2H(^2\Sigma^+)$. However, these product channels have exothermicities of 25−40 kcal/mol, i.e., much lower than those for the C_4H_4 + H and $C_2H_3 + C_2H_2$ products, and thus are not expected to contribute into the reaction with any significance. For example, the decomposition of INT4 to $C_3H_3(^2B_1) + CH_2(^3B_1)$ would result in the energy loss of ∼91 kcal/mol, while the barrier for the H loss producing p1 is only ∼47 kcal/mol and on these grounds the $C_3H_3(^2B_1) + CH_2(^3B_1)$ products can be safely ruled out. Decompositions of INT2, INT5, INT6, and INT8 with an H atom loss would lead to high-lying cyclic isomers of C_4H_4 and therefore are unlikely. The CH_2 group loss from INT5 gives a three-member ring structure of C_3H_3, ∼40 kcal/mol higher in energy than the most stable isomer of the propargyl radical,[23b] so that this channel also would not contribute into the reaction. It is worth mentioning that nonadiabatic effects are not expected to be important for this reaction as the lowest excited states of the major products, C_4H_4 + H and $C_2H_3 + C_2H_2$, lie significantly higher in energy than their ground electronic states, for instance, by 41.5, 69.1, and 88.1 kcal/mol for triplet states of H_2CCCCH_2, $H_2CCHCCH$,[31] and acetylene,[32] respectively, and by 57.2 kcal/mol for the $1^2A''$ state of C_2H_3.[32]

3.3. Most Favorable Channels of the $C(^3P_j) + C_3H_5(X\ ^2A_1)$ Reaction. On the basis of the calculated PES illustrated in Figure 1, we can now summarize the most energetically favorable channels of the $C(^3P_j) + C_3H_5(X\ ^2A_1)$ reaction. The carbon atom addition to a terminal CH_2 of the allyl radical leads to a metastable intermediate INT1, which immediately isomerizes to buta-1,3-dien-4-yl INT3, and the latter decomposes to either p1 + H or $C_2H_3 + C_2H_2$ (p3): $C(^3P_j) + C_3H_5(X\ ^2A_1) \rightarrow$ INT1 → INT3 → p1 + H/$C_2H_3 + C_2H_2$. Alternatively, INT3 can rearrange to buta-1,2-dien-4-yl INT4, which can lose H atoms from two different positions giving C_4H_4 p1 or p2: $C(^3P_j) + C_3H_5(X\ ^2A_1) \rightarrow$ INT1 → INT3 → INT4 → p1/p2 + H. In addition, INT4 can rearrange to but-2-yn-1-yl INT7, which in turn decomposes to p2 + H. If at the initial step the attacking carbon atom adds between two CH_2 group, the bicyclic INT2 intermediate is formed, and then the preferable reaction pathway is isomerization of the latter consequently to INT4 (via INT5) and INT3: $C(^3P_j) + C_3H_5(X\ ^2A_1) \rightarrow$ INT2 → INT5 → INT4 → INT3. Decomposition of INT4 and INT3 again results in the p1, p2, or p3 products. On the basis of this consideration, vinylacetylene + H, butatriene + H, and vinyl radical + acetylene can be predicted as the major reaction products. Our RRKM calculations described in section 3.4 allow us to support this qualitative conclusion with calculated relative branching ratios.

Let us also consider the most favorable pathways for decomposition of various low-lying isomers of the C_4H_5 radical. For buta-1,3-dien-4-yl, they are the following: INT3 → $H_2CCHCCH$ + H with the barrier of 37.9 kcal/mol; INT3 → $C_2H_3 + C_2H_2$ (43.4 kcal/mol barrier); and INT3 → INT4 → $H_2CCHCCH$ + H and INT3 → INT4 → H_2CCCCH_2 + H, both with the highest barrier of 47.4 kcal/mol for the INT3→INT4 isomerization step. Buta-1,2-dien-4-yl can dissociate by the following pathways: INT4 → $H_2CCHCCH$ + H over the 46.8 kcal/mol barrier, INT4 → H_2CCCCH_2 + H (55.5 kcal/mol barrier), and INT4 → INT7 → H_2CCCCH_2 + H with the highest barrier of 54.1 kcal/mol relative to INT4 for the last step. But-2-yn-1-yl INT7 fragments to H_2CCCCH_2 + H overcoming the barrier of 55.9 kcal/mol or to $H_2CCHCCH$ + H via INT4 with the highest barrier of 55.7 kcal/mol for the INT7→INT4 rearrangement. Finally, the most favorable pathway for the but-1-yn-3-yl decomposition is INT9 → $H_2CCHCCH$ + H with the 46.3 kcal/mol barrier.

Recent photofragment translational spectroscopy studies of buta-1,2-diene at 193 nm by Neumark and co-workers[33] showed C_4H_5 radicals as primary photodissociation products. They undergo secondary decomposition if their translational energy is lower than 7 kcal/mol, i.e., the 7 kcal/mol cutoff was observed in the translation energy distribution of the C_4H_5 products. According to our calculations,[34] three isomers of C_4H_5 can be formed from buta-1,2-diene, but-2-yn-1-yl INT7, buta-1,2-dien-4-yl INT4, and but-1-yn-3-yl INT9. The overall available energies for INT7, INT4, and INT9 after primary photodissociation of the parent buta-1,2-diene molecule at 193 nm were computed as 63.0, 61.2, and 60.7 kcal/mol.[34] On the other hand, the minimal internal energies these radicals need to possess in order to overcome the barriers along the most favorable decomposition pathways are 55.7 kcal/mol for but-2-yn-1-yl, 46.8 kcal/mol for buta-1,2-dien-4-yl, and 46.3 kcal/mol for but-1-yn-3-yl. Therefore, the minimal translational energies these isomers can have in order to survive secondary dissociation are 7.3, 14.4, and 14.4 kcal/mol, respectively. This finding is in a good agreement with the translational energy cutoff observed in experiment.[33]

3.4. Rate Constants and Product Branching Ratios. Calculated rate constants for various unimolecular reaction steps are collected in Table 2, while relative branching ratios for different product channels are presented in Table 3. The calculations were carried out assuming zero collision energy, i.e., zero internal energy in excess of the reactants zero-point level. One can see that three rate constants, k_2 (INT1→INT3), k_{10} (INT6→INT7), and k_{13} (INT8→INT9) are higher than 10^{13} s^{-1}, indicating that the basic assumptions of the RRKM theory of a statistical distribution of the vibrational energy over all modes can break down, as redistribution of the internal energy occurs on a picosecond scale. Such high unimolecular rates can lead to nonstatistical behavior of the system. INT1 is a metastable intermediate and the rate constant calculations simply show that it should immediately isomerize to INT3, while its rearrangements to INT2 and INT4 are about an order of magnitude slower. INT6 and INT8 are unlikely to play any significant role in the reaction because since both can be produced from INT2 by the INT2 → INT6 → INT8 mechanism but the rate constant k_7(INT2→INT6) is 336 times lower than k_5(INT2→INT5). Hence, we expect that possible non-RRKM

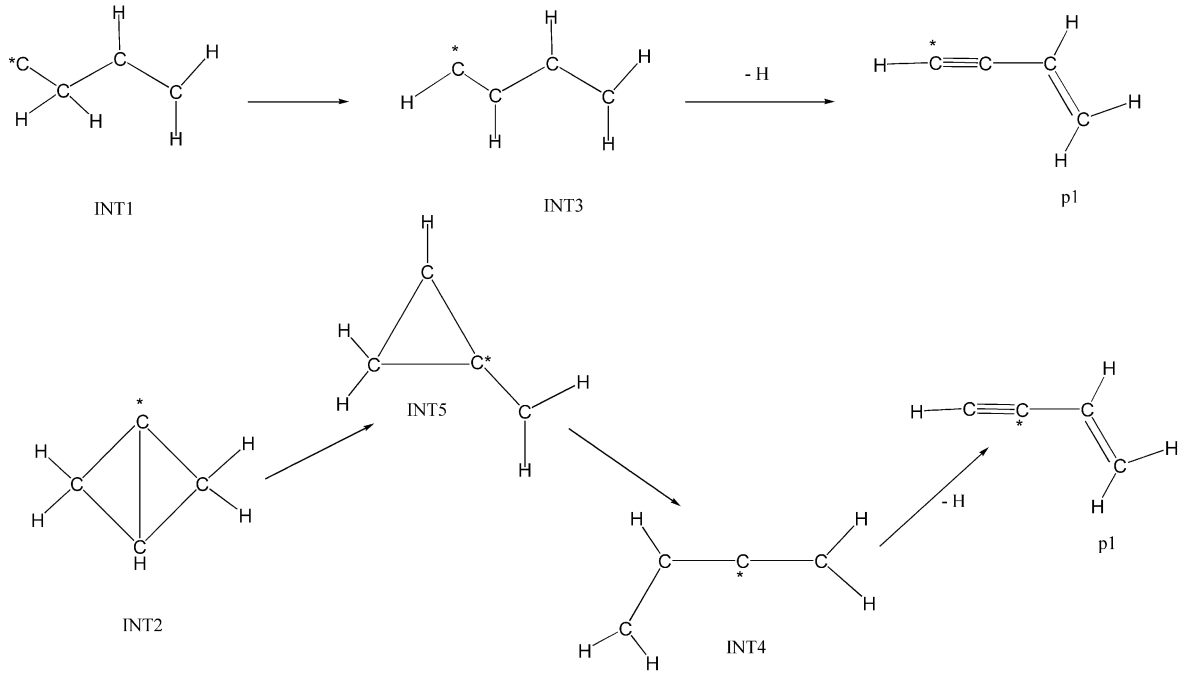

Figure 4. Formation of distinct vinylacetylene isomers (p1) via the reaction of carbon atoms with the allyl radical.

TABLE 2: Microcanonical Rate Constants (s^{-1}) for Various Unimolecular Reaction Channels

channel	rate constant
k_1: INT1 → INT2	2.86×10^{12}
k_{-1}: INT2 → INT1	3.03×10^{12}
k_2: INT1 → INT3	2.72×10^{13}
k_{-2}: INT3 → INT1	1.57×10^{10}
k_3: INT1 → INT4	2.18×10^{12}
k_{-3}: INT4 → INT1	3.78×10^{8}
k_4: INT3 → INT4	4.86×10^{10}
k_{-4}: INT4 → INT3	1.46×10^{10}
k_5: INT2 → INT5	2.91×10^{12}
k_{-5}: INT5 → INT2	9.11×10^{9}
k_6: INT4 → INT5	3.65×10^{11}
k_{-6}: INT5 → INT4	7.00×10^{12}
k_7: INT2 → INT6	8.66×10^{9}
k_{-7}: INT6 → INT2	8.48×10^{8}
k_8: INT3 → INT9	1.70×10^{9}
k_{-8}: INT9 → INT3	1.70×10^{8}
k_9: INT4 → INT7	1.67×10^{11}
k_{-9}: INT7 → INT4	1.38×10^{10}
k_{10}: INT6 → INT7	2.38×10^{13}
k_{-10}: INT7 → INT6	3.28×10^{9}
k_{11}: INT6 → INT8	3.37×10^{9}
k_{-11}: INT8 → INT6	2.85×10^{9}
k_{12}: INT7 → INT9	1.34×10^{4}
k_{-12}: INT9 → INT7	5.43×10^{4}
k_{13}: INT8 → INT9	3.81×10^{13}
k_{-13}: INT9 → INT8	2.51×10^{10}
k_{14}: INT3 → p1	1.79×10^{12}
k_{15}: INT3 → p3	6.91×10^{12}
k_{16}: INT4 → p1	4.10×10^{12}
k_{17}: INT4 → p2	9.84×10^{10}
k_{18}: INT7 → p2	5.34×10^{9}
k_{19}: INT9 → p1	6.72×10^{10}
k_{20}: INT8 → p6	1.23×10^{11}
k_{21}: INT9 → p8	7.48×10^{7}

behavior for the INT1 → INT3, INT6 → INT7, and INT8 → INT9 rearrangements should not affect our results.

Calculations of branching ratios (Table 3) demonstrate that they strongly depend on the initial ratio of concentrations of intermediates INT1 and INT2. Both of them can be formed without a barrier from $C(^3P_j) + C_3H_5(X\ ^2A_1)$, and the initial branching between two highly exothermic pathway is a dynamical problem. To solve it, one has to generate PES for the carbon atom approach toward a CH_2 group in allyl to from INT1 and between two CH_2 fragments to produce INT2. Dynamics calculations using these surfaces can give an answer concerning the branching ratios in the $C(^3P_j) + C_3H_5(X\ ^2A_1) \rightarrow$ INT1/INT2 reaction. In the present work, we simply consider various initial concentrations of INT1 and INT2 and obtain the product branching ratios depending on these initial concentrations. Assuming that only INT1 is produced when $C(^3P_j)$ attacks the allyl radical, the calculated p1 ($H_2CCHCCH + H$) and p3 ($C_2H_3 + C_2H_2$) branching ratios are 29.8% and 69.8%, respectively, and for the opposite limiting case (100% of INT2) the p1 and p3 branching ratios change to 62.4% and 35.7%, respectively. Butatriene + H (p2) gives only a minor contribution, 0.4−1.9%. The branching ratios for the other products, such as, for example, $c\text{-}C_3H_2 + CH_3$ and $l\text{-}C_3H + CH_4$, are negligibly small. These results indicate that the branching ratio of vinylacetylene plus hydrogen and of vinyl plus acetylene should strongly depend on the collision impact parameter. For instance, small impact parameters (the carbon atom attacks H_2CCHCH_2 near its center of mass) should favor the formation of INT2 and increase the contribution of vinylacetylene. Alternatively, large-impact-parameter collisions (the attack far from the center of mass) should lead to the formation of INT1 and increase the relative yield of $C_2H_3 + C_2H_2$.

TABLE 3: Calculated Product Branching Ratios (%) for the $C(^3P_j) + C_3H_5(X\ ^2A_1)$ Reaction at Various Initial Concentrations of INT1 and INT2

INT1	INT2	p1 ($H_2CCHCCH + H$)	p2 ($H_2CCCCH_2 + H$)	p3 ($C_2H_3 + C_2H_2$)
100	0	29.8	0.4	69.8
90	10	33.0	0.6	66.4
80	20	36.3	0.7	63.0
70	30	39.5	0.9	59.6
60	40	42.8	1.0	56.2
50	50	46.1	1.2	52.7
40	60	49.3	1.4	49.3
30	70	52.6	1.5	45.9
20	80	55.9	1.6	42.5
10	90	59.1	1.8	39.1
0	100	62.4	1.9	35.7

The dependence of the p1 and p3 branching ratios on the starting concentrations of INT1 and INT2 can be understood based on the potential energy diagram shown in Figure 1 and the calculated rate constants. If INT1 is produced, it will immediately rearrange to INT3 and the latter will decompose mostly to vinyl + acetylene, $k_{15}(\text{INT3}\rightarrow\text{p3}) = 6.91 \times 10^{12}\ s^{-1}$, and to a lesser extent to vinylacetylene + H, $k_{14}(\text{INT3}\rightarrow\text{p1}) = 1.79 \times 10^{12}\ s^{-1}$. On the other hand, if INT2 is formed, it isomerizes first to INT5, then to INT4, and only then to INT3. Since the INT4→INT3 isomerization is rather slow, $k_{-4} = 1.46 \times 10^{10}\ s^{-1}$, before INT3 is reached INT4 can dissociate predominantly to p1, $k_{16}(\text{INT4}\rightarrow\text{p1}) = 4.10 \times 10^{12}\ s^{-1}$, and to a little extent to butatriene + H (p2).

Our previous ab initio/RRKM studies of other chemical reactions, for example, photodissociation of the propargyl radical,[23b] carbonyl cyanide,[35] 1,2- and 1,3-butadienes,[34] and the $O(^1D) + C_3H_6$ reaction,[36] demonstrated that this method is able to provide product branching ratios with the accuracy within 5% as compared to experiment for the reaction channels occurring on the ground state PES. The results presented in this section are expected to have a rather qualitative character as for some reaction steps a non-RRKM behavior is probable and the branching ratios strongly depend on initial concentrations of INT1 and INT2 after addition of the carbon atom to the allyl radical. A direct dynamics study would be able to provide more quantitative results. Nevertheless, the statistical calculations are useful for qualitative prediction of the reaction products and for future comparison with the results of the dynamics calculations, which can demonstrate the effects of nonstatistical behavior.

3.5. Implications to Interstellar Chemistry. Both the allyl radical reactant and the vinylacetylene and butatriene reaction products have been included in chemical reaction networks modeling the hydrocarbon chemistry in the atmospheres of the giant planets Jupiter and Saturn.[37] Current photochemical models suggest that the allyl radical presents the photodissociation product of propylene (C_3H_6), whereas vinylacetylene and butatriene might be formed through photodissociation of various C_4H_6 isomers.[34,38] Surprisingly, the reaction of carbon atoms, which may be present as transient species in hydrocarbon rich planetary and satellite atmospheres, with the allyl radical has never been included as an open channel to synthesize vinylacetylene and/or butatriene in these extreme environments. Considering the principle of microscopic reversibility, we must also have a closer look at the vinyl plus acetylene reaction channel. In the reverse reaction, vibrationally excited vinyl radicals—formed, for instance, by photodissociation of ethylene—may also react with acetylene through an entrance barrier of 6.0 kcal/mol via intermediate INT3 to open the vinylacetylene plus atomic hydrogen channel in a reaction exoergic by 5.0 kcal/mol. Therefore, our computational results infer that the reaction of atomic carbon with the allyl radical and binary collisions of the vinyl radical with acetylene can form C_4H_4 isomers in hydrocarbon rich atmospheres of planets and their moons in our solar system. The actual identification of these isomers in the atmosphere of Saturn's moon Titan is a task of the Cassini−Huygens currently en route to the Saturnian system.

4. Conclusions

Ab initio G2M(MP2)//B3LYP/6-311G** calculations of PES for the reaction of the ground-state atomic carbon with the allyl radical demonstrate that $C(^3P_j)$ can add without a barrier either to a terminal CH_2 group of $C_3H_5(X\ ^2A_1)$ to form a metastable intermediate INT1 or between two CH_2 groups to produce INT2. INT1 immediately isomerizes to buta-1,3-dien-4-yl INT3, which can decompose to C_4H_4 (vinylacetylene) + H or to the vinyl + acetylene products. INT3 can also rearrange to 1,2-dien-4-yl INT4 by a 1,2-hydrogen migration, and INT4 fragments by the H atom loss to vinylacetylene or butatriene. The alternative pathway from the reactants to INT4 involves ring opening in the bicyclic intermediate INT2 leading to a three-member ring intermediate INT5 followed the ring opening in the latter. 1,2-dien-4-yl INT4 can also rearrange to but-2-yn-1-yl INT7, which in turn decomposes to butatriene + H. The other reaction channels are much less favorable according to the calculated energies and rate constants.

Vinylacetylene + H (p1) and vinyl radical + acetylene (p3) are predicted to be the major reaction products, while butatriene + H are the minor products. Calculated branching ratios of p1 and p3 are strongly dependent on the initial branching between the initial intermediates INT1 and INT2 and vary between p1/p3 = 29.8/69.8 if 100% of INT1 is produced in the $C(^3P_j) + C_3H_5(X\ ^2A_1)$ collision and 62.4/35.7 if 100% of INT2 are initially formed. Since INT1 and INT2 are produced by collisions with different impact parameters, we conclude the p1/p3 branching ratio would be influenced by the impact parameter; collisions with small impact parameters would favor the formation of INT2 and, hence, the production of vinylacetylene + H, while high-impact-parameter collisions would lead to INT1 and enhance the $C_2H_3 + C_2H_2$ products.

Note, however, that our RRKM calculations alone do not necessarily reveal the actual reaction mechanisms involved. The RRKM theory, for instance, assumes a complete energy randomization in the decomposing intermediate of a bimolecular reaction before the latter fragments. However, crossed-beam studies of $C(^3P_j)$/1,2-butadiene[39] and $(^3P_j)/CD_3CCH$,[40] as well as crossed-beam studies of the reactions of electronically excited carbon atoms $C(^1D_2)$ with acetylene, ethylene, and methylacetylene,[41] revealed discrepancies between the calculated and the experimentally observed product distributions. Additionally, future experiments should account for distinct microchannels which can lead to the same vinylacetylene reaction product (p1) (Figure 4). Microchannel 1 leads to the vinylacetylene isomer via intermediates INT1 and INT3. Here, the attacking carbon atom, denoted with an asterisk, is found at the terminal position of the carbon chain at the acetylenic bond of p1. On the other hand, an addition of atomic carbon at the central carbon atom of the allyl radical via INT2, INT5, and INT4 gives a vinylacetylene isomer in which the carbon atom is located at the second carbon of the acetylenic group. Nevertheless, our investigations provide guidance on reaction intermediates and on enthalpies of formation of the products. Therefore, prospective crossed-beam experiments and computations of the pertinent potential energy surfaces are highly complimentary to expose the reaction dynamics of complicated, polyatomic reactions comprehensively which can lead to the formation of the astrophysically important vinylacetylene isomer in the interstellar medium and in hydrocarbon rich planetary atmospheres.

Acknowledgment. A.M.M. thanks Academia Sinica and National Science Council of Taiwan, R.O.C., (Grant NSC 91-2113-M-001-029) for the financial support.

References and Notes

(1) Keene, J.; Young, K.; Phillips, T. G.; Buttgenbach, T. H., Carlstrom, J. E. *Astrophys. J.* **1993**, *415*, L131.

(2) van der Keen, W. E. C. J.; Huggins, P. J.; Matthews, H. E. *Astrophys. J.* **1998**, *505*, 749.

(3) Ingalls, J. G.; Chamberlin, R. A.; Bania, T. M.; Jackson, J. M.; Lane, A. P.; Stark, A. A. *Astrophys. J.* **1997**, *479*, 296.
(4) Wilson, C. D. *Astrophys. J. Lett.* **1997**, *487*, 49.
(5) Young, K. *Astrophys. J.* **1997**, *488*, L157.
(6) Sofia, U. J.; Cardelli, J. A.; Guerin, K. P.; Meyer, D. M. *Astrophys. J. Lett.* **1997**, *482*, 105.
(7) White, G. J.; Sandell, G. *Astron. Astrophys.* **1995**, *299*, 179.
(8) Hung, W. C.; Huang, M. L.; Lee, Y. C.; Lee, Y. P. *J. Chem. Phys.* **1995**, *103*, 9941.
(9) Weissman, M.; Benson, S. W. *Prog. Energy Combust. Sci*. **1989**, *15*, 273.
(10) Linder, R. E.; Winters, D. L.; Ling, A. C. *Can. J. Chem*. **1976**, *54*, 1405.
(11) Tsang, W. *Int. J. Chem. Kinet.* **1978**, *10*, 1119.
(12) Kaiser, R. I.; Mebel, A. M. *Int. Rev. Phys. Chem.* **2002**, *21*, 307. Kaiser, R. I., *Chem. Rev.* **2002**, *102*, 1309.
(13) Becke, A. D. *J. Chem. Phys.* **1993**, *98*, 5648.
(14) Lee, C.; Yang, W.; Parr, R. G. *Phys. Rev. B* **1988**, *37*, 785.
(15) Mebel, A. M.; Morokuma, K.; Lin, M. C. *J. Chem. Phys.* **1995**, *103*, 414.
(16) Purvis, G. D.; Bartlett, R. J. *J. Chem. Phys*. **1982**, *76*, 1910. (b) Scuseria, G. E.; Janssen, C. L.; Schaefer, H. F., III *J. Chem. Phys*. **1988**, *89*, 7382. (c) Scuseria, G. E.; Schaefer, H. F., III *J. Chem. Phys*. **1989**, *90*, 3700; Pople, J. A.; Head-Gordon, M.; Raghavachari, K. *J. Chem. Phys*. **1987**, *87*, 5968.
(17) Frisch, M. J.; Trucks, G. W.; Schlegel, H. B.; Scuseria, G. E.; Robb, M. A.; Cheeseman, J. R.; Zakrzewski, V. G.; Montgomery, J. A., Jr.; Stratmann, R. E.; Burant, J. C.; Dapprich, S.; Millam, J. M.; Daniels, A. D.; Kudin, K. N.; Strain, M. C.; Farkas, O.; Tomasi, J.; Barone, V.; Cossi, M.; Cammi, R.; Mennucci, B.; Pomelli, C.; Adamo, C.; Clifford, S.; Ochterski, J.; Petersson, G. A.; Ayala, P. Y.; Cui, Q.; Morokuma, K.; Malick, D. K.; Rabuck, A. D.; Raghavachari, K.; Foresman, J. B.; Cioslowski, J.; Ortiz, J. V.; Baboul, A. G.; Stefanov, B. B.; Liu, G.; Liashenko, A.; Piskorz, P.; Komaromi, I.; Gomperts, R.; Martin, R. L.; Fox, D. J.; Keith, T.; Al-Laham, M. A.; Peng, C. Y.; Nanayakkara, A.; Gonzalez, C.; Challacombe, M.; Gill, P. M. W.; Johnson, B.; Chen, W.; Wong, M. W.; Andres, J. L.; Head-Gordon, M.; Replogle, E. S.; Pople, J. A. GAUSSIAN 98, revision A.9; Gaussian, Inc.: Pittsburgh, PA, 1998.
(18) MOLPRO is a package of ab initio programs written by Werner, H.-J.; Knowles, P. J., with contributions from Almlöf, J.; Amos, R. D.; Deegan, M. J. O.; Elbert, S. T.; Hampel, C.; Meyer, W.; Peterson, K.; Pitzer, R.; Stone, A. J.; Taylor, P. R.; Lindh, R.
(19) Eyring, H.; Lin, S. H.; Lin, S. M. *Basic Chemical Kinetics*; Wiley: New York, 1980.
(20) Robinson, P. J.; Holbrook, K. A. *Unimolecular Reactions*; Wiley: New York, 1972.
(21) Steinfield, J. I.; Francisco, J. S.; Hase, W. L. *Chemical Kinetics and Dynamics*; Prentice Hall: Engelwood Cliffs, NJ, 1999.
(22) Stein, S. E.; Rabinovitch, B. S. *J. Phys. Chem.* **1973**, *58*, 2438.
(23) Kaiser, R. I.; Ochsenfeld, C.; Stranges, D.; Head-Gordon, M.; Lee, Y. T. *Discuss. Faraday Soc.* **1998**, *109*, 183. (b) Nguyen, T. L.; Mebel, A. M.; Kaiser, R. I. *J. Phys. Chem. A* **2001**, *105*, 3284. (c) Nguyen, T. L.; Mebel, A. M.; Lin, S. H.; Kaiser, R. I. *J. Phys. Chem. A* **2001**, *105*, 11549.
(24) Kaiser, R. I.; Sun, W.; Suits, A. G.; Lee, Y. T. *J. Chem. Phys.* **1997**, *107*, 8713. (b) Le, T. N.; Mebel, A. M.; Kaiser, R. I. *J. Comput. Chem.* **2001**, *22*, 1522.
(25) Parker, C. L.; Cooksy, A. L. *J. Phys. Chem. A* **1998**, *102*, 6186. (b) Parker, C. L.; Cooksy, A. L. *J. Phys. Chem. A* **1999**, *103*, 2160.
(26) *NIST Chemistry Webbook*, NIST Standard Reference DataBase Number 69; July 2001 Release (http://webbook.nist.gov/chemistry/).
(27) Mebel, A. M.; Jackson, W. M.; Chang, A. H. H.; Lin S. H. *J. Am. Chem. Soc.* **1998**, *120*, 5751.
(28) Mebel, A. M.; Morokuma, K.; Lin, M. C. *J. Chem. Phys.* **1995**, *103*, 3440.
(29) Kim, G.-S.; Nguyen, T. L.; Mebel, A. M.; Lin, S. H.; Nguyen, M. T. *J. Phys. Chem. A* **2003**, *107*, 1788.
(30) Kurosaki, Y.; Takayanagi, T. *J. Chem. Phys.* **2000**, *113*, 4060.
(31) Mebel, A. M.; Kaiser, R. I.; Lee, Y. T. *J. Am. Chem. Soc.* **2000**, *122*, 1776. (b) Balucani, N.; Mebel, A. M.; Lee, Y. T.; Kaiser, R. I. *J. Phys. Chem. A* **2001**, *105*, 9813.
(32) Mebel, A. M.; Chen, Y.-T.; Lin, S. H. *Chem. Phys. Lett.* **1997**, 19.
(33) Robinson, J. C.; Sun, W.; Harris, S. A.; Qi, F.; Neumark, D. M. *J. Chem. Phys.* **2001**, *115*, 8359.
(34) Lee, H. Y.; Kislov, V. V.; Lin, S. H.; Mebel, A. M.; Neumark, D. M. *Chem. Eur. J.* **2003**, *9*, 726.
(35) Lee, H. Y.; Mebel, A. M.; Lin, S. H. *Int. J. Quantum Chem.* **2002**, *90*, 566.
(36) Wang, C. C.; Lee, Y. T.; Yang, X.; Nguyen, T. L.; Mebel, A. M. *J. Chem. Phys.* **2002**, *116*, 8292
(37) Yung, Y. K.; DeMoore, W. B. *Photochemistry of Planetary Atmospheres*; Oxford University Press: Oxford, 1999.
(38) Robinson, J. C.; Harris, S. A.; Sun, W.; Sveum, N. E.; Neumark, D. N. *J. Am. Chem. Soc.* **2002**, *124*, 10211.
(39) Balucani, N.; Lee, H. Y.; Mebel, A. M.; Lee, Y. T.; Kaiser, R. I. *J. Chem. Phys.* **2001,** *15*, 5107.
(40) Kaiser, R. I.; Mebel, A. M.; Lee, Y. T.; Chang, A. H. H. *J. Chem. Phys*. **2001**, *115*, 5117.
(41) Kaiser, R. I.; Mebel, A. M.; Lee, Y. T. *J. Chem. Phys* **2001**, *114***,** 231.